14th Australasian Fluid Mechanics Conference
Adelaide University, Adelaide, Australia
10-14 December 2001

Measurements of Turbulent Prandtl Number of a Heated Square Jet

Chua L.P., Li Y. F., Zhou T. and Yu C.M.S.

School of Mechanical and Production Engineering
Nanyang University of Singapore, Nanyang Avenue,
Singapore 639798, SINGAPORE
E-mail: mlpchua@ntu.edu.sg

Abstract

The paper presents the mean and root mean square velocity and temperature distributions of a heated square jet flow into a stagnant environment. The Reynolds shear stress, heat flux and turbulent Prandtl number were also measured by means of a three-wire (i.e. a cold wire in front of an X-wire) probe. It is found that the mean velocity and temperature have reached self-preservation nearly immediately after the potential core. The Reynolds shear stress and heat flux, have however achieved the self-similarity at 30 *De* and 35 *De* respectively. The distribution of Prandtl number here is about constant in the range of $0<y/Ly<0.8$, and then increase steeply. The finding has suggested that it may have incurred some inaccuracy in the computation fluid mechanics results by assuming a constant turbulent Prandtl number in the jet.

Introduction

Noncircular jets were identified as an efficient technique of passive flow control that allows significant improvements of performance such as reducing combustion instabilities and undesired emissions, noise suppression, and thrust vector control, at a relatively low cost and rely solely on changes in the geometry of the nozzle. It was then not unexpected that the noncircular jets have been the topic of extensive research in the last fifteen years [6].

However, among the noncircular jets, there were relatively less experimental measurements on square jet besides the studies of Tsuchiya et al [11], Quinn and Militzer [9], Gutmark et al [7] and Grinstein et al [5]. The measurements of Tsuchiya et al [11] and Gutmark et al [7], nevertheless, were mainly on the rectangular and triangular jets respectively, with square jet was just a small part. There are also lack of the temperature measurements especially the heat flux distributions in the literature with most of the measurements are on the velocity alone except Tsuchiya et al [11].

A definition sketch of the nozzle, velocity and temperature profiles are shown in Figure 1a. Three-wire probe (as shown in Figure 1b) is used to measure the Reynolds shear stress and heat flux.

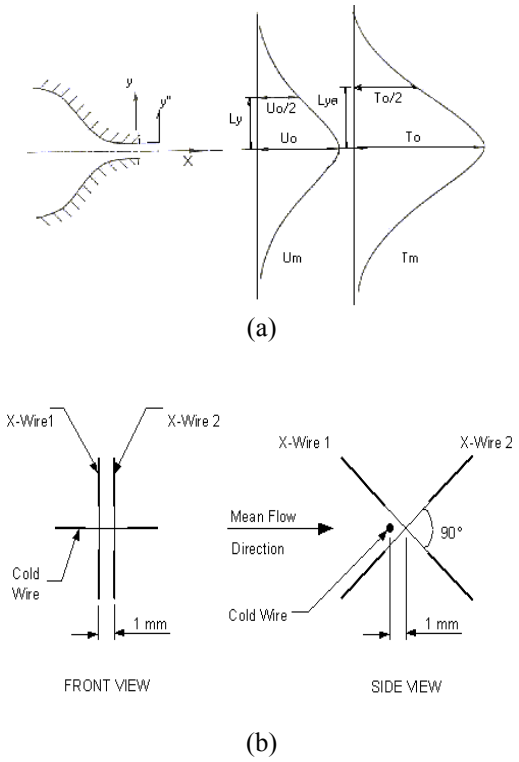

Figure 1. (a) Definition sketch for present jet and (b) three- wire probe

The main objective of the paper is thus to present the measurements of heat fluxes and hence a subsequent determination of turbulent Prandtl number at the far field of the contour square jet. The turbulent Prandtl number, which is an important parameter in computational fluid mechanics, is usually assumed a constant value in the calculation.

Experimental method

The jet exit velocity U_j was set at 31±0.5m/s and the corresponding Reynolds number was 57500. The contoured nozzle was designed according to the incompressible axis-symmetric potential flow theory [10], in order to (i) avoid flow separation from taking place in the construction, and (ii) achieve uniform flow at the exit. Installed between the blower and nozzle were a divergence section, settling chamber of size 250mm X 250mm X

250mm, screens and honeycomb section to convey the flow and reduce turbulence. The air is heated with a 1 kW electrical coil element situated at the inlet of the blower and the temperature of the heated air can be controlled by means of thermostat through a thermocouple installed in the air duct. The heating element is placed at the inlet of the blower so that it can ensure a better mixing of the heated air prior to the entry into the settling chamber. Further, the entire jet assembly was wrapped in three layers of fibre-glass as further increment in insulation layers was found to have no significant improvement in preventing heat loss from the heated jet and to eliminate the buoyancy effect [8]. The temperature at the nozzle exit was set at 20±0.5°C above the ambient air and it takes about an hour to have a uniform temperature distribution along both the horizontal and vertical axes at the jet exit.

For the three-wire measurements, the cold wire (ϕ1.2μm Wollaston Pt 10%-Rh, length ≈ 1.5mm) is located about 1mm in front of the center of the X-wire as shown in Figure 1b; both X-wire 1 and 2 are hot wire (ϕ5μm Wollaston Pt 10%-Rh, length ≈ 1.0mm) connected to a constant temperature anemometer (CTA) module operating at an overheat ratio of 1.5. The included angle of the probe was about 90° and the separation between the two wires was about 1.0mm. The probe was mounted onto a dial height gauge fixed to a traversing mechanism capable of traveling in three perpendicular directions (x, y and z axes).

The hot wire was calibrated prior to each measurement set in the potential core with reference to a pitot-static tube connected to a pressure transducer. For the three-wire measurements, voltages from the CTA and pressure transducer were digitized by a 12-bit analog-to-digital converter before input into a computer for processing. After calibration constants were computed using the least squares method, they were then fed into the second part of the computer program which converted hot wire voltages into velocities. Besides obtaining the usual calibration constants, the X-wire probe was calibrated for velocity and yaw in the potential core of the jet, the range of yaw angles being -15° to 15° in 3° steps. Voltages from three-wire were passed through low-pass filters before digitizing, using National Instrument model into a computer. The sampling frequency is double the cut off frequency (1600Hz) and the recording time is 15 seconds for the three channels (three-wire). Digitized hot wire and cold wire voltages were converted to velocity and temperature respectively. The statistical parameters such as mean, root mean square and the cross correlation of the u and v as well as v and θ were obtained using the program written in Matlab.

Using the method of propagation of errors, the experimental uncertainty in $\overline{uv}/U_o^2$, $\overline{v\theta}/U_oT_0$ and turbulent Prandtl number were correspondingly estimated as ±6.5%, ±5.4% and ±7.1%.

Results and discussion

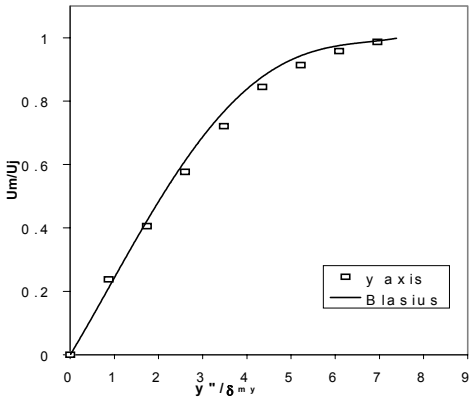

Figure 2. Boundary layer velocity profile at nozzle exit

Figure 2 illustrates good agreement of the jet boundary layer with Blasius' solution for a flat plate. The normalizing scale is the boundary layer momentum thickness which was evaluated to be 0.115mm (δ_{my}) for y axis.

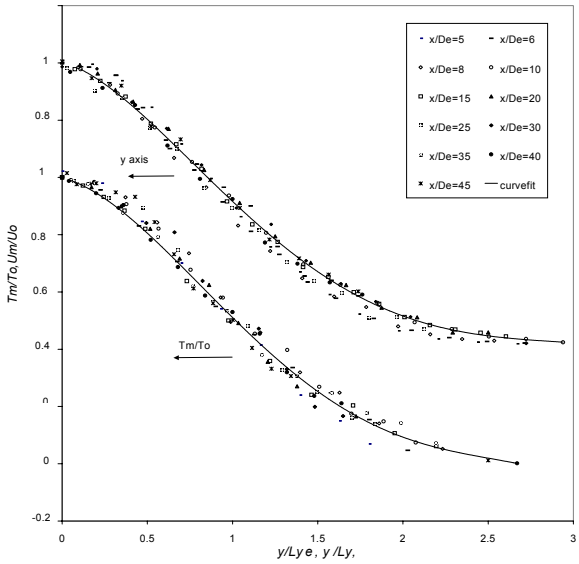

Figure 3. Mean temperature and velocity from 5De to 45De

The mean velocity and temperature profiles in the interaction and self-preservation regions in the range $5 \le x/De \le 45$ are displayed in Figure 3. Here, the local centerline mean velocity U_o, local centerline mean temperature To, velocity half-width L_y and temperature half-width $L_{y\theta}$ are the normalizing co-ordinates. As evident in the figure, the mean velocity and temperature distributions collapse onto a single curve indicating that U_m and T_m reached self-preservation at the end of potential core, that is $x = 5De$.

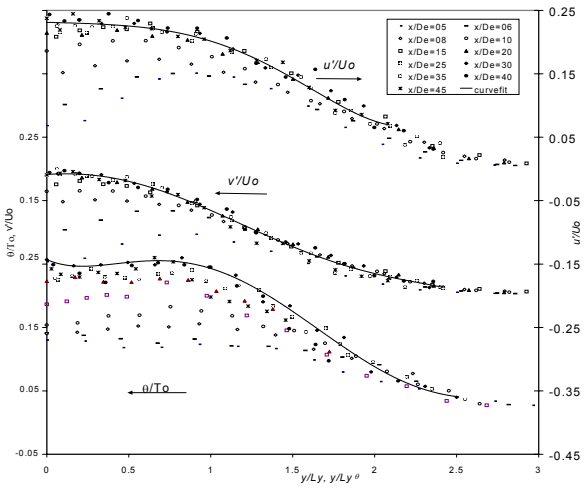

Figure 4. Root mean square of temperature (θ) and velocity along x direction (u') and y direction (v')

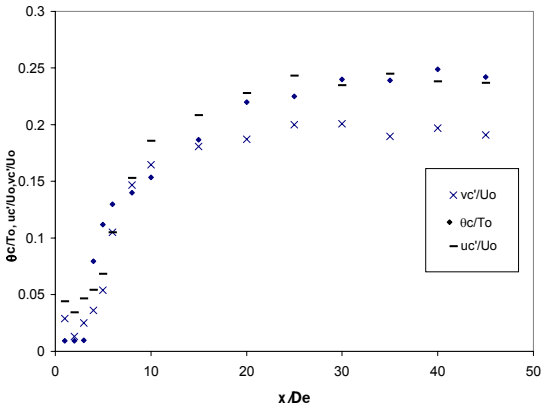

Figure 5. Streamwise distributions of centerline root mean square of temperature, axial and lateral velocity

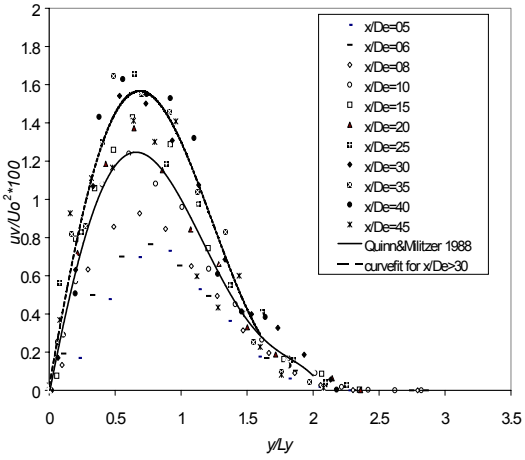

Figure 6. Streamwise distribution of Reynolds shear stress $\overline{uv}$ along y axis

Figure 4 shows the distributions of u'/U_o , v'/U_o, and θ/T_o respectively. It can be observed that both the distributions increased from 5*De* and reached a self-preservation at 25*De* and 20*De* respectively for u'/U_o and v'/U_o. The shape of the distributions is changing from saddle like with the peak at about y/Ly=1 at 5*De* to Gaussian Shape with the peak slowly shifts towards the centerline. Unlike v'/U_o which monotonically decreases from the centerline once it reaches the self-preservation state, the distributions of u'/U_o have shown a small peak at about 0.5*Ly*. The distributions of u'/U_o have reached a peak of about 0.24 which is higher than the peak of about 0.2 for v'/U_o. These results indicate that the fluctuations of the axial velocity have higher kinetic energy than the lateral velocity. Comparing with the root mean square velocity distributions, the profiles of the θ/T_o at the small streamwise location are relatively flat without any obvious peak until 8*De*. The root mean square temperature distributions reach a self-preservation at about 20*De* and the profiles exhibit a vague peak at about $y/Ly\theta$=1, this is again different from the v'/U_o with monotonous decrease from the jet centerline.

Figure 5 shows the streamwise distributions of the centerline axial and lateral root mean square velocities and temperature. Both of the centerline root mean square axial velocity and temperature distributions have reached an asymptotic value of 0.24 at 25*De*, while the lateral root mean square velocity has about the constant values of 0.19 at the similar streamwise locations.

Figure 6 shows the distributions of normalized Reynolds shear stress $\overline{uv}$ at various x/De locations. Note that the absolute values of $\overline{uv}$ are presented in Figure 6, as they are symmetrical about the centerline. Also shown in the figure is the distributions obtained by Quinn and Militzer [8] at about 13De and a best fit curve for the Reynolds shear stresses higher than 30De.

The Reynolds shear stress has increased from 5*De* and reached the self-preservation at about 30*De*. The location of the Reynolds shear stress peak has also shifted from about 1.0*Ly* to 0.8*Ly*. The peak of Quinn and Militzer [8] distribution has only reached 0.012 at about 0.7*Ly*, it may not be totally unexpected as the measurements were done at about 13*De* and should not have reached the self-preservation state at this low streamwise location.

The heat flux distribution which is normalized by both the local centerline mean velocity U_o and temperature T_o is shown in Figure 7. It can be observed that the normalized heat flux distribution has reached self-preservation at about 35*De* in the figure. Both the Reynolds shear stress and heat flux distributions have shown some scatter especially at the high streamwise location for example 45*De*, this is due to the fast decay of mean velocity and temperature at these locations. Further, the jet is a high turbulence intensity flow, for instance, at 40*D*e, the u'/U_m (v'/U_m) and θ/T_m are about 0.24 (0.20) and 0.25 at the jet axis as shown earlier in Figure 5. At the jet

half-width, the values of u'/U_m, v'/U_m and θ/T_m have increased to 0.50, 0.34 and 0.39 respectively. Such high fluctuations coupled with the fact that flow reversal has started to occur at the half-width location as Chua and Antonia [2] have found in the circular jet. All these have contributed to the difficulty in measurements. As the velocity vector angle at these locations may have over 90^0, the included angle of 120^0 X-wire may be more suitable for the present measurements [1].

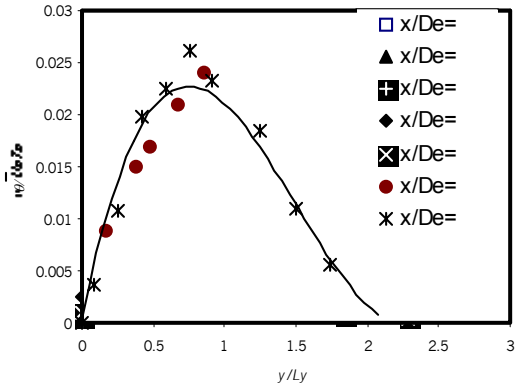

Figure 7. Streamwise distribution of heat flux $\overline{v\theta}$ along *y*-axis

With the measured Reynolds shear stress and the heat flux, the eddy diffusivity for momentum and heat can be obtained as

$$\nu_T = -\frac{\overline{uv}}{(\partial U_m / \partial y)} \tag{1}$$

and

$$\alpha_T = -\frac{\overline{v\theta}}{(\partial T_m / \partial y)} \tag{2}$$

Consequently, turbulent Prandtl number Pr_T defined as the ratio of eddy diffusivities for momentum and heat can be written as

$$p_{r_T} = \frac{\nu_T}{\alpha_T} \tag{3}$$

Note that both $\partial U_m / \partial y$ and $\partial T_m / \partial y$ were obtained from Figure 3 with the 4th order polynomial fit to the U_m/U_o and the T_m/T_o distributions. In both cases, the limiting values of these quantities at y/Ly=0 were obtained using L'Hopital rule. The distributions of turbulent Prandtl number Pr_T are demonstrated in Figure 8. Also shown in the figure is the distributions of Prandtl number of circular jet [3] plotted for comparison. The figure shows that Prandtl number is not constant across the jet. Rather, the quantity maintains at about a constant value of 0.6 before rising steeply after *y/Ly*=1.0. This has implied that the turbulent Prandtl number Pr_T, which is an important parameter for similarity solutions of non-isothermal square jets, should not be taken as a constant. Within the region *y/Ly*=1.0, the error in obtaining the mean temperature and heat flux profiles using computation fluid mechanics of the square jet may be negligible, whereas significant deviation from the actual flow may arise if Pr_T is taken as the same constant value beyond the range in the simulation.

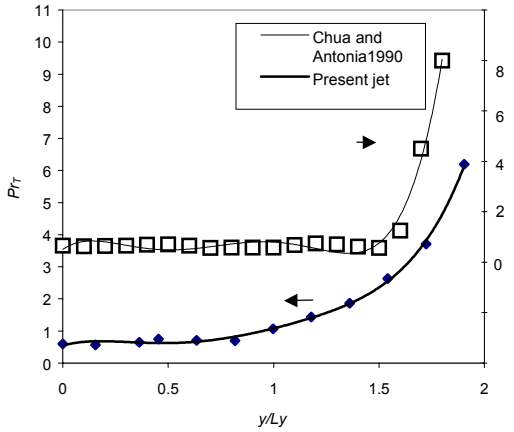

Figure 8. Variations of turbulent Prandtl number along *y* axis

Conclusion

The initial flow condition of the square jet under investigation was found to be laminar. The mean velocity and temperature has reached self-preservation immediately after the potential core. The Reynolds shear stress and heat flux have reached self-preservation respectively at about 30*De* and 35*De*. The distribution of turbulent Prandtl number has indicated that it might have incurred some errors in the computation fluid mechanics results if Pr_T was treated as a constant value throughout the whole *y* locations.

Reference

1. Browne L.W.B., Antonia R.A. and Chua L.P., "Velocity vector cone angle in turbulent flows", *Expt. In Fluids*, **8**, 13-16, 1989.

2. Chua L.P. and Antonia R. A., "Flow reversal and intermittency of a turbulent jet", *AIAA J.*, **27**,1494-1499, 1989. 1.

3. Chua L.P. and Antonia R. A., "Turbulent Prandtl number in a circular jet", *J. Heat Mass Transfer.* Vol.33, 334-339, 1990.

4. Chua L.P. and Goh E.Y., "Design and eliminating the buoyancy effect of a heated circular jet," *Int. Comm. In Heat & Mass Transf.*, **21**, 629-639, 1994.

5. Grinstein F. F., Gutmark E. J. and Parr T., "Near field dynamics of subsonic free square jets. A computiaitonal and experimental study", *Phys. of Fluids*, **7**, 1483-1497, 1995.

6. Gutmark E. J. and Grinstein F. F., Flow control with noncircular jets, *Annu. Rev. Fluid Mech.*, **31**, 239-272, 1999.

7. Gutmark E. J., Schadow T. P., Parr T. P., Hanson-Parr D.M. and Wilson K.J., Noncircular jets in combustion systems, *Expt. In Fluids*, **7**, 248-258, 1989.

8. Quinn, W. R. and Militzer, J., Experimental and numerical study of a turbulent free square jet, *Physics of Fluids*, **31**, 1017-1025, 1988.

9. Quinn W. R., Streamwise evolution of a square jet cross section, *AIAA J.*, **30**, 2852-2857, 1992.

10. Tsien H.S., "On the design of the contraction cone for a wind tunnel," *J. Aeron. Sc.*, **10**, 68-70, 1943.

11. Tsuchiya Y., Horikoshi C. and Sato T., On the spread of rectangular jets, *Expt. In Fluids*, **4**, 197-204, 1986.